

Cite this: *Nanoscale*, 2011, **3**, 4074

www.rsc.org/nanoscale

COMMUNICATION

Hierarchical protonated titanate nanostructures for lithium-ion batteries†

Yanyan Zhang,^{‡a} Yuxin Tang,^{‡a} Shengyan Yin,^a Zhiyuan Zeng,^a Hua Zhang,^a Chang Ming Li,^b Zhili Dong,^a Zhong Chen^{*a} and Xiaodong Chen^{*a}

Received 22nd May 2011, Accepted 29th July 2011

DOI: 10.1039/c1nr10522a

3D protonated titanate nanoflowers synthesized by an organic-free and cost-effective facile method exhibit a high reversible capacity, excellent cycling performance, and a remarkable rate capability when they worked as anode electrode materials for lithium-ion batteries.

Lithium-ion batteries (LIBs) have been widely accepted as one of the most promising energy storage devices, which cover a diversity of applications with the requirements of high energy density, high rate capability, and excellent cycle performance.¹ Much effort has been focused on designing and synthesizing nanostructured electrode materials with high surface area and short diffusion paths for lithium ions and electrons.^{1b,e,2} Recently, hierarchical porous nanostructures have attracted increasing attention due to their higher surface area accessible to the electrolyte, short path length for lithium ions and electrons, and sufficient space to accommodate the volume change.³ For instance, it has been shown that electrodes made of super-structured materials such as V₂O₅,^{3a} SnO,^{3b} SnO₂,^{3c} TiO₂-RuO₂,^{3d} Co₃O₄,^{3e} and Si-C^{3f} displayed remarkable electrochemical properties, such as high capacity and good reversibility. Up to now, various methodologies, such as chemical vapor deposition (CVD),^{3f} atomic layer deposition (ALD),⁴ hydrothermal process,⁵ and self-assembly,^{3a-c,e,g} have been developed to fabricate the particular hierarchical nanostructures. However, these approaches are largely time/energy consuming, as well as environmentally malign, seriously hindering the large-scale practical application. Herein, we reported an organic-free and cost-effective facile method to synthesize protonated titanate nanomaterials with the novel hierarchical structures, which exhibited remarkable electrochemical performance as anode electrode materials for LIBs.

There are four reasons for us to choose protonated titanate as anode electrode materials: (1) it possesses a layered crystal structure with large interlayer spacing (*ca.* 0.8 nm), which could accommodate the intercalated lithium ions while maintaining the crystal structure;⁶

(2) it has the intrinsic safety characteristics compared to the commercial graphite anode suffering from the electroplating of lithium;^{6b,7} (3) nanostructured protonated titanate materials have exhibited remarkable electrochemical performance (*e.g.*, large initial discharge capacity of 282 mA h g⁻¹ at the current density of 240 mA g⁻¹ for protonated titanate nanotubes (PTNFs));⁸ and (4) it is composed of three abundant elements (hydrogen, titanium and oxygen) in the world, hence it is cost-effective and viable for industry.

First, we synthesized the sodium titanate nanoflowers (NaTNFs) by means of an electrochemical spark discharge spallation (ESDS) process within 20 min.⁹ The detailed procedure is described in the Experimental section (ESI†). The X-ray diffraction (XRD) pattern of NaTNFs (iii) of Fig. 1a) is indexed to body-centered orthorhombic titanate (JCPDS no. 47-0124), which is made up of two-dimensional (2D) sheets composed of edge sharing TiO₆ octahedra.^{5b} The broad peaks at $2\theta = 9.2^\circ$, 24.6° , 28.5° , 34.9° , 38.8° , 48.3° , and 62.0° correspond basically to the (200), (110), (310), (301), (501), (020), and

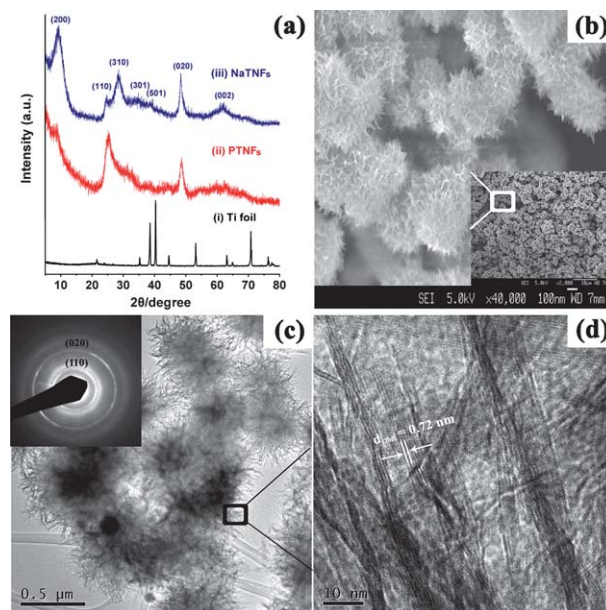


Fig. 1 (a) XRD patterns of the (i) titanium foil, (ii) PTNFs, and (iii) NaTNFs prepared by the ESDS method; (b) FE-SEM image of PTNFs; (c) TEM image of PTNFs; and (d) high resolution TEM image of PTNFs. The inset in (c) is a selected area electron diffraction pattern of PTNFs.

^aSchool of Materials Science and Engineering, Nanyang Technological University, 50 Nanyang Avenue, Singapore 639798. E-mail: chenxd@ntu.edu.sg; aszchen@ntu.edu.sg

^bSchool of Chemical and Biomedical Engineering, Nanyang Technological University, 70 Nanyang Drive, Singapore 637457

† Electronic supplementary information (ESI) available: Experimental section, analytical methods, electrochemical measurements, and supplementary results. See DOI: 10.1039/c1nr10522a

‡ These authors have contributed equally to this work.

(002) planes of the orthorhombic titanate phase.^{5b,10} Thus, the structure of NaTNFs should be assigned to layered $\text{Na}_x\text{H}_{2-x}\text{Ti}_2\text{O}_5$, which has similar host layers to those in the lepidocrocite-type titanate, but with different cations.¹¹

Then, we obtained the protonated titanate nanoflowers (PTNFs) by immersing the as-prepared NaTNF samples into 0.1 M HCl solution for one day in order to have the complete ion exchange of sodium ions by protons. Energy dispersive X-ray spectroscopy (EDS) measurement (Fig. S1†) provides direct evidence of the complete conversion from NaTNFs to PTNFs, since there is no sodium element signal in the PTNF samples. Furthermore, it is noteworthy that the XRD pattern of the PTNF samples ((ii) of Fig. 1a) has a relatively low intensity compared to that of the as-prepared NaTNF samples, although the morphology does not change when NaTNFs were converted to PTNFs. This is due to the poor crystallinity of the protonated titanate after the ion exchange,¹² which suggests the presence of a slight structural transformation from a sodium hydrogen titanate to a hydrogen titanate ($\text{H}_2\text{Ti}_2\text{O}_5$).^{5a,13} Furthermore, the rings in selected area electron diffraction (SAED) (inset in Fig. 1c) suggest that PTNFs are polycrystalline. Two separated diffraction rings corresponding to the (110) and (020) planes of PTNFs are observed (inset in Fig. 1c), and the rest of the SAED rings are very obscure. These results are consistent with the XRD results of PTNFs. From transmission electron microscopy (TEM) and scanning electron microscopy (SEM) images (Fig. 1b and c), we can clearly observe that the three-dimensional (3D) PTNFs consist of individually aligned 2D titanate nanosheets, which are bundled perpendicularly to the central core to form a hierarchical morphology. The size of flower structures ranges from 0.4 μm to 1.5 μm , and the interlayer distance of PTNFs is about 0.72 nm, as shown in the high resolution TEM image (Fig. 1d). The interlayer distance is consistent with the literature report on the protonated titanate materials.⁵ Additionally, the 3D hierarchical PTNFs are highly porous (Fig. 1c), and the Brunauer–Emmett–Teller (BET) surface area is 406.41 $\text{m}^2 \text{g}^{-1}$, which is much higher than the reported data of titanate nanomaterials.⁶

From the above description, we can see that the method and process to synthesize such 3D hierarchical PTNFs are environment-benign and economic. Furthermore, it is noted that the hierarchical porous structures composed of nanometre-sized sheets and micro-scale flowers, layered nanostructures, and high specific surface area in PTNF samples would be the favourable configuration to help enhance the electrolyte diffusion and lithium ions intercalation. Therefore, PTNFs could be suitable for the application as anode electrode materials for LIBs.

In a proof-of-concept experiment, coin cells (2032) with a metallic lithium counter electrode were used to evaluate the electrochemical performance of the as-prepared PTNF samples. The capacity and cycle performance were evaluated by galvanostatic charge/discharge measurements at a current density of 50 mA g^{-1} with a potential window from 1.00 to 3.00 V (*versus* Li/Li⁺) (Fig. 2a). The smoothly sloping feature (without any potential plateau) of the curve indicates that intermediate phases are not formed during lithium intercalation/extraction processes.^{8f,12} Typically, the high initial discharge capacity of 419 mA h g^{-1} is achieved, and the reversible charge capacity is 302 mA h g^{-1} for the first process. An irreversible capacity loss of 28% may be due to the trapping of lithium ions inside the titanate framework and the solid electrolyte interface (SEI) layers forming in the interface of the electrode and the electrolyte. The lithium-ion storage tends to be stable after four cycles for the Coulombic

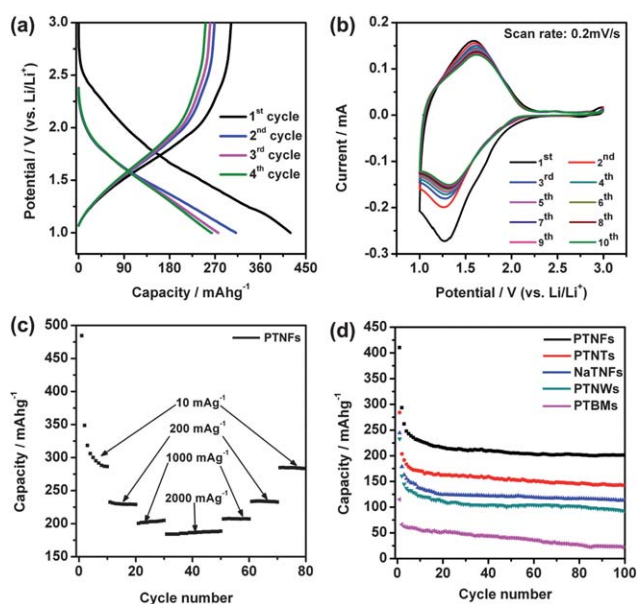


Fig. 2 Electrochemical performance of the titanate materials: (a) the first four discharge/charge cycles of a PTNF electrode at a current density of 50 mA g^{-1} ; (b) cyclic voltammograms of a PTNF electrode in 1 M LiPF₆ + ethylene carbonate/diethyl carbonate (1/1, v/v) at a scan rate of 0.2 mV s^{-1} ; (c) galvanostatic cycling performance of a PTNF electrode at different discharge rates; and (d) the cycle performances of all samples at a current density of 50 mA g^{-1} .

efficiency reaches 95%. Cyclic voltammograms (CV) experiments were further conducted to evaluate the electrochemical performance of the PTNF electrode at a scan rate of 0.2 mV s^{-1} over the voltage range of 1.00–3.00 V (Fig. 2b). In the CV curves, we only observed one pair of broad redox peaks, which is well in agreement with the sloping property in the discharge/charge profiles in Fig. 2a. The peak at 1.33 V corresponds to the process of insertion of lithium ions.^{8d,e} It is also noted that the peaks become wider with the cycling, which may be due to the reason that it is more difficult for lithium ions inserting into the PTNF electrode because of the trapping of lithium ions inside the PTNF framework. After four cycles, there is no clear change in the CV curves, suggesting the equilibrium of the inserting and releasing lithium ions.

In addition, the PTNF electrodes exhibit very good rate capability operating at various current densities between 10 mA g^{-1} and 2000 mA g^{-1} . Cycle performances of PTNF electrodes at different current densities of 10 mA g^{-1} , 200 mA g^{-1} , 1000 mA g^{-1} and 2000 mA g^{-1} are shown in Fig. 2c. It can be clearly observed that PTNFs show excellent capacity retention and give out a quite high capacity of 484 mA h g^{-1} at the current density of 10 mA g^{-1} , and the capacity decreases to 200 mA h g^{-1} when the current density increases to 1000 mA g^{-1} . Furthermore, a reversible capacity of 184 mA h g^{-1} is obtained at an even higher current density of 2000 mA g^{-1} , nicely confirming the short diffusion path length in our ultrathin titanate nanosheets. Moreover, the discharge performance remains stable in the following corresponding back stages and the specific capacities are resumed when the rates are reduced back to lower current density. The above electrochemical results of PTNF samples indicate that the as-prepared PTNFs have an intensive potential as a candidate of anode materials with high reversible capacity, good cycle performance, and high rate discharge/charge capability. It mostly may be

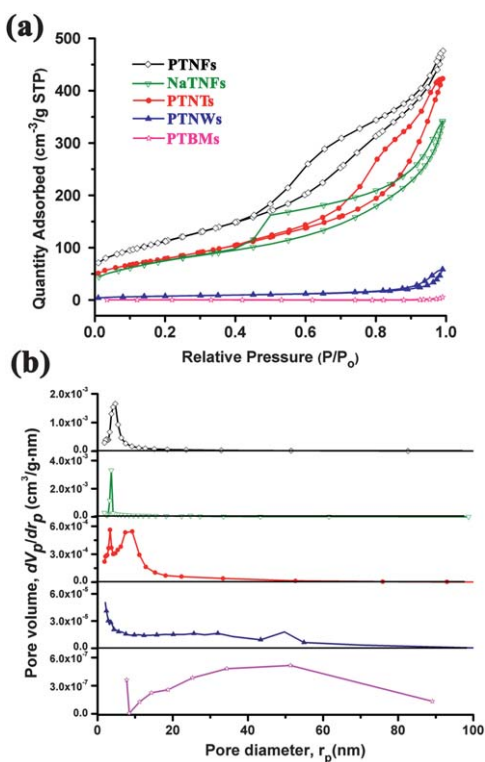


Fig. 3 (a) Nitrogen (N_2) sorption isotherms and (b) pore-size distributions of PTNFs (\square), NaTNFs (∇), PTNTs (\bullet), PTNWs (\blacktriangle), and PTBMs (\star).

due to the unique hierarchical architecture composed of countless nanometre-sized sheets and each sheet can serve as the host of lithium ions. Specifically, the as-prepared PTNFs with larger surface area ($406.41 \text{ m}^2 \text{ g}^{-1}$) facilitate the electrolyte access to the electrode and allow the lithium ions to insert into the electrode quickly.

For comparison, we also prepared PTBMs *via* the pyrosynthesis method,¹⁴ protonated titanate nanowires (PTNWs) and PTNTs by the hydrothermal approach.¹⁵ Detailed experimental conditions with the XRD data and morphology (Fig. S2†) of these materials are described in the ESI†. Fig. 2d illustrates the cycle performance of all titanate samples at a current density of 50 mA g^{-1} . It is evident that electrodes made of PTNTs, PTNWs, NaTNFs, and PTNFs all exhibit good cycling performance during lithium ions insertion and extraction processes. This is mainly attributed to the accommodation of the volume change during the lithium ions storage process benefiting from the intrinsic layered structure of titanate. It is also noted that the cyclic performance of PTBMs is deteriorated compared to others. Moreover, after 100 cycles, the PTNF electrode

Table 1 BET surface area, pore volume and pore size of different samples

Samples	BET surface area/ $\text{m}^2 \text{ g}^{-1}$	Pore volume/ $\text{cm}^3 \text{ g}^{-1}$	Average pore size/nm
PTNFs	406.41	0.75	5.9
PTNTs	284.63	0.60	7.9
NaTNFs	277.52	0.52	7.5
PTNWs	27.70	0.092	13.5
PTBMs	2.07	0.0072	46.1

exhibits the highest reversible capacity at $\sim 200 \text{ mA h g}^{-1}$ compared with other titanate nanomaterials (the reversible capacities of PTNTs, PTNWs, NaTNFs and PTBMs are 142, 93, 114 and 22 mA h g^{-1} , respectively). Such high performance of PTNFs may be mainly owing to the synergetic effect of their components: the large amount of pore channels ($0.75 \text{ cm}^3 \text{ g}^{-1}$) and 2D nanosheets to provide a negligible diffusion time for the electrolyte, higher specific surface areas to allow more lithium ions to get access to the layered host matrix, while the micro-scale flower-like spheres guarantee the good stability. In addition, the morphology of the PTNFs after 100 cycles is retained, which is confirmed by the FESEM image shown in the ESI (Fig. S3†).

The measurements on the specific surface area, pore volume, and average pore size of these samples further confirmed the above arguments. The typical nitrogen sorption isotherms and Barrett–Joyner–Halenda (BJH) pore size distribution curves of the above-mentioned samples are shown in Fig. 3, and the data are summarized in Table 1. Compared with PTNTs, NaTNFs, PTNWs, and PTBMs, PTNFs have relatively larger surface area ($406.41 \text{ m}^2 \text{ g}^{-1}$), which is benefiting from the large pore volume ($0.75 \text{ cm}^3 \text{ g}^{-1}$) and narrow pore size distribution (maximum value of 4.4 nm). In addition, the result of specific surface area is closely tallying with the tendency of their electrochemical performance. The larger surface area could offer more contact surface for the electrolyte/electrode and would be convenient for the lithium ions to insert into the electrode sufficiently, so the electrochemical performance would be better.

In conclusion, 3D porous hierarchical PTNFs have been successfully synthesized by the combination of a fast and facile ESDS method with a simple ion exchange. These hierarchical PTNFs exhibit a high reversible capacity, excellent cycling performance, and remarkable rate capacity, when they worked as the anode materials for LIBs. These extraordinary electrochemical properties are mainly attributed to the synergistic effect of the porous structure and the particular hierarchical structure composed of the nanometre-sized sheets and micro-scale flowers. While the porous structure and the ultra-thin nanosheets provide higher specific surface area and shorter diffusion lengths for the lithium ions and electrons, the micro-scale flowers maintain the interior structure and guarantee good stability.

Acknowledgements

This work was supported by National Research Foundation of Singapore (CREATE and MEWR651/06/160).

References

- (a) M. R. Palacin, *Chem. Soc. Rev.*, 2009, **38**, 2565–2575; (b) Y. Wang and G. Z. Cao, *Adv. Mater.*, 2008, **20**, 2251–2269; (c) F. Cheng, Z. Tao, J. Liang and J. Chen, *Chem. Mater.*, 2008, **20**, 667–681; (d) H. Li, Z. X. Wang, L. Q. Chen and X. J. Huang, *Adv. Mater.*, 2009, **21**, 4593–4607; (e) Y. G. Guo, J. S. Hu and L. J. Wan, *Adv. Mater.*, 2008, **20**, 2878–2887; (f) M. Holzapfel, H. Buqa, W. Scheifele, P. Novak and F. M. Petrat, *Chem. Commun.*, 2005, 1566–1568.
- (a) J. Chen and F. Y. Cheng, *Acc. Chem. Res.*, 2009, **42**, 713–723; (b) A. S. Arico, P. Bruce, B. Scrosati, J. M. Tarascon and W. Van Schalkwijk, *Nat. Mater.*, 2005, **4**, 366–377.
- (a) A. M. Cao, J. S. Hu, H. P. Liang and L. J. Wan, *Angew. Chem., Int. Ed.*, 2005, **44**, 4391–4395; (b) J. J. Ning, T. Jiang, K. K. Men, Q. Q. Dai, D. M. Li, Y. J. Wei, B. B. Liu, G. Chen, B. Zou and G. T. Zou, *J. Phys. Chem. C*, 2009, **113**, 14140–14144; (c) L. Y. Jiang, X. L. Wu, Y. G. Guo and L. J. Wan, *J. Phys. Chem. C*, 2009, **113**, 14213–14219; (d) Y. G. Guo, Y. S. Hu, W. Sigle and

- J. Maier, *Adv. Mater.*, 2007, **19**, 2087–2091; (e) X. Wang, X. L. Wu, Y. G. Guo, Y. T. Zhong, X. Q. Cao, Y. Ma and J. N. Yao, *Adv. Funct. Mater.*, 2010, **20**, 1680–1686; (f) A. Magasinski, P. Dixon, B. Hertzberg, A. Kvit, J. Ayala and G. Yushin, *Nat. Mater.*, 2010, **9**, 353–358; (g) S. Y. Yin, Y. Y. Zhang, J. H. Kong, C. J. Zou, C. M. Li, X. H. Lu, J. Ma, F. Y. C. Boey and X. D. Chen, *ACS Nano*, 2011, **5**, 3831–3838.
- 4 C. Bae, Y. Yoon, W. S. Yoon, J. Moon, J. Kim and H. Shin, *ACS Appl. Mater. Interfaces*, 2010, **2**, 1581–1587.
- 5 (a) Y. Takezawa and H. Imai, *Small*, 2006, **2**, 390–393; (b) C. Wu, L. Lei, X. Zhu, J. Yang and Y. Xie, *Small*, 2007, **3**, 1518–1522.
- 6 (a) G. H. Du, Q. Chen, R. C. Che, Z. Y. Yuan and L. M. Peng, *Appl. Phys. Lett.*, 2001, **79**, 3702–3704; (b) D. V. Bavykin, J. M. Friedrich and F. C. Walsh, *Adv. Mater.*, 2006, **18**, 2807–2824; (c) Y. Lan, X. P. Gao, H. Y. Zhu, Z. F. Zheng, T. Y. Yan, F. Wu, S. P. Ringer and D. Y. Song, *Adv. Funct. Mater.*, 2005, **15**, 1310–1318.
- 7 D. V. Bavykin and F. C. Walsh, *Eur. J. Inorg. Chem.*, 2009, 977–997.
- 8 (a) Q. Chen, W. Z. Zhou, G. H. Du and L. M. Peng, *Adv. Mater.*, 2002, **14**, 1208–1211; (b) J. R. Li, Z. L. Tang and Z. T. Zhang, *Chem. Phys. Lett.*, 2006, **418**, 506–510; (c) H. Zhang, X. P. Gao, G. R. Li, T. Y. Yan and H. Y. Zhu, *Electrochim. Acta*, 2008, **53**, 7061–7068; (d) J. R. Li, Z. L. Tang and Z. T. Zhang, *Electrochem. Commun.*, 2005, **7**, 62–67; (e) J. R. Li, Z. L. Tang and Z. T. Zhang, *Chem. Mater.*, 2005, **17**, 5848–5855; (f) M. D. Wei, K. W. Wei, M. Ichihara and H. S. Zhou, *Electrochem. Commun.*, 2008, **10**, 1164–1167; (g) A. R. Armstrong, G. Armstrong, J. Canales, R. Garcia and P. G. Bruce, *Adv. Mater.*, 2005, **17**, 862–865; (h) B. L. Wang, Q. Chen, J. Hu, H. Li, Y. F. Hu and L. M. Peng, *Chem. Phys. Lett.*, 2005, **406**, 95–100.
- 9 Y. X. Tang, Y. K. Lai, D. G. Gong, K.-H. Goh, T.-T. Lim, Z. L. Dong and Z. Chen, *Chem.–Eur. J.*, 2010, **16**, 7704–7708.
- 10 J. Q. Huang, Z. Huang, W. Guo, M. L. Wang, Y. G. Cao and M. C. Hong, *Cryst. Growth Des.*, 2008, **8**, 2444–2446.
- 11 (a) R. Z. Ma, K. Fukuda, T. Sasaki, M. Osada and Y. Bando, *J. Phys. Chem. B*, 2005, **109**, 6210–6214; (b) R. Z. Ma, Y. Bando and T. Sasaki, *Chem. Phys. Lett.*, 2003, **380**, 577–582.
- 12 H. Zhang, G. R. Li, L. P. An, T. Y. Yan, X. P. Gao and H. Y. Zhu, *J. Phys. Chem. C*, 2007, **111**, 6143–6148.
- 13 Y. B. Mao, M. Kanungo, T. Hemraj-Benny and S. S. Wong, *J. Phys. Chem. B*, 2006, **110**, 702–710.
- 14 T. P. Feist and P. K. Davies, *J. Solid State Chem.*, 1992, **101**, 275–295.
- 15 (a) D. Wu, J. Liu, X. N. Zhao, A. D. Li, Y. F. Chen and N. B. Ming, *Chem. Mater.*, 2006, **18**, 547–553; (b) X. M. Sun and Y. D. Li, *Chem.–Eur. J.*, 2003, **9**, 2229–2238.